

DOCUMENT CONTROL SHEET

	ORIGINATOR'S REF. NLR-TP-2003-191	SECURITY CLASS. Unclassified				
ORIGINATOR National Aerospace Laboratory NLR, Amsterdam, The Netherlands						
TITLE GARTEUR (AD) AG-26: Navier-Stokes computations of 3D transonic flow for a wing/fuselage configuration						
PRESENTED AT CEAS Aerospace Aerodynamics Research Conference, Cambridge (UK), 10-12 June, 2002						
AUTHORS F.J. Brandsma	DATE May 2003	<table border="1" style="width: 100%; border-collapse: collapse;"> <tr> <td style="width: 50%;">PP</td> <td style="width: 50%;">REF</td> </tr> <tr> <td style="text-align: center;">27</td> <td style="text-align: center;">16</td> </tr> </table>	PP	REF	27	16
PP	REF					
27	16					
ABSTRACT In this paper the work carried out within the GARTEUR Action Group (AD) AG-26 on the validation of computational fluid dynamics (CFD) methods for transonic flow around transport type of aircraft is presented. The participants of AG-26 are Aerospatiale (AS), BAE SYSTEMS (BAe), EADS (DASA), NLR, ONERA and Saab. They simulated the flow around the AS28G wing/body configuration of Aerospatiale for a transonic design and an transonic off-design condition with their CFD methods based on the Reynolds averaged Navier-Stokes equations using a common computational grid that made available by BAe. Various turbulence models have been employed. A code-to-code comparisons has been made on the basis of computed aerodynamic force and moment coefficients, pressure distributions, skin friction coefficients, and boundary layer profiles. The pressure distributions have been compared with the experimental data obtained in the ONERA S1-Modane wind tunnel. Agreement between the computational and experimental pressure distributions is generally good except for the shock position and the region close to the wing trailing edge. There is a significant variation in computed aerodynamic force coefficients (attributed to variation in predicted shock position and separation locations) which could not systematically be related to the numerical method and turbulence models employed for this study. Even though it was expected that the off-design would be a more difficult case to predict, the variation in the computational results is more or less the same for both test cases. It is concluded among other things that the common computational grid did not allow to distinguish between discretisation error and modelling errors and it is recommended for future CFD validation studies to adopt a grid convergence approach rather than a common grid strategy.						



NLR-TP-2003-191




**GARTEUR (AD) AG-26:
Navier-Stokes computations of 3D transonic
flow for a wing/fuselage configuration**

F.J. Brandsma

This report is based on a presentation held at CEAS Aerospace Aerodynamics Research Conference, Cambridge (UK), 10-12 June, 2002.

This report may be cited on condition that full credit is given to NLR and the authors.

Customer: National Aerospace Laboratory NLR
Working Plan number: A.1.B.7
Owner: National Aerospace Laboratory NLR
Division: Fluid Dynamics
Distribution: Unlimited
Classification title: Unclassified
May 2003

Approved by author: 	Approved by project manager: 	Approved by project managing department: 
--	--	---



Summary

In this paper the work carried out within the GARTEUR Action Group (AD) AG-26 on the validation of computational fluid dynamics (CFD) methods for transonic flow around transport type of aircraft is presented. The participants of AG-26 are Aerospatiale (AS), BAE SYSTEMS (BAe), EADS (DASA), NLR, ONERA and Saab. They simulated the flow around the AS28G wing/body configuration of Aerospatiale for a transonic design and an transonic off-design condition with their CFD methods based on the Reynolds averaged Navier-Stokes equations using a common computational grid that made available by BAe. Various turbulence models have been employed. A code-to-code comparisons has been made on the basis of computed aerodynamic force and moment coefficients, pressure distributions, skin friction coefficients, and boundary layer profiles. The pressure distributions have been compared with the experimental data obtained in the ONERA S1-Modane wind tunnel. Agreement between the computational and experimental pressure distributions is generally good except for the shock position and the region close to the wing trailing edge. There is a significant variation in computed aerodynamic force coefficients (attributed to variation in predicted shock position and separation locations) which could not systematically be related to the numerical method and turbulence models employed for this study. Even though it was expected that the off-design would be a more difficult case to predict, the variation in the computational results is more or less the same for both test cases. It is concluded among other things that the common computational grid did not allow to distinguish between discretisation error and modelling errors and it is recommended for future CFD validation studies to adopt a grid convergence approach rather than a common grid strategy.



Contents

1	Introduction	7
2	Test cases	7
3	CFD Methods	9
4	Computational grid	10
5	Discussion of results	11
5.1	Pressure distributions	13
5.2	Skin friction distributions	15
5.3	Boundary layer profiles	18
5.4	Aerodynamic coefficients	20
6	Conclusions	23
7	Acknowledgement	25
8	References	25

(26 pages in total)



List of Symbols

b	Wing half span
c	Local wing chord
C_D	Drag coefficient
C_L	Lift coefficient
C_L^{exp}	Lift coefficient obtained from the wind tunnel experiment
C_L^{CFD}	Lift coefficient obtained from the numerical simulations
C_{MY}	Pitching moment coefficient
C_p	Pressure coefficient
g	Variable in $k - g$ turbulence model
k	Turbulent kinetic energy ($k - g$, $k - \omega$, and $k - \epsilon$ turbulence models)
ν_T	Turbulent Viscosity
u	Streamwise velocity component
x	Streamwise coordinate
y	Spanwise coordinate
z_D	Dimensionless distance to wing surface or wake centerline
α	Angle of incidence
ϵ	Dissipation of turbulent kinetic energy ($k - \epsilon$ turbulence model)
ω	Specific dissipation rate of turbulent kinetic energy ($k - \omega$ turbulence models)

List of abbreviations

AD	Aero Dynamics
AG	Action Group
AS	Aerospatiale
AS28G	Aerospatiale wind tunnel model
AVTAC	Advanced Viscous Flow Simulation Tools for Complete Civil Aircraft Design
BAe	British Aerospace
BL	Baldwin & Lomax (turbulence model)
CFD	Computational Fluid Dynamics
DASA	Daimler-Benz Aerospace Airbus
EADS	European Aeronautic Defence and Space Company
EC	European Committee
GARTEUR	Group for Aeronautical Research and Technology in Europe



NLR	Nationaal Lucht- en Ruimtevaartlaboratorium
ONERA	Office National d'Etudes et Recherches Aerospatiales
RaNS	Reynolds-averaged Navier-Stokes



1 Introduction

The main purpose of the GARTEUR (AD) Action Group 26 has been to validate flow computation methods based on the Reynolds-averaged Navier-Stokes equations for the prediction of transonic flow physics on transport aircraft wings in design and off-design conditions. The participants involved in this Action Group are Aerospatiale (further referred to as AS), BAE SYSTEMS (further referred to as BAe), EADS (further referred to under its former name DASA), NLR, ONERA, and Saab. The Action Group can be considered as the follow-up of the Action Group (AD) AG-17 Ref 6), that verified computational methods based on the Euler equations for three-dimensional subsonic and transonic, inviscid flow around complex configurations. The present Action Group started its work with observation that the CFD methods based on the Navier-Stokes equations available to the research institutes and industries participating in GARTEUR have matured to such extent that a validation of the methods and in particular the turbulence models employed within these methods is expected to be valuable. Detailed validation studies for transport aircraft configuration both on a basis of code-to-code comparisons as well as on comparison of experimental data in a collaborative effort like this Action Group is of great importance for the participants to get confidence in their CFD methods. Moreover, the results of the validation exercise give a good indication about the potential of present day Navier-Stokes methods to be used as valuable tools in the design of modern transport aircraft. The AS28G wing-fuselage model has been selected as a well-suited configuration for the computational effort within AG-26, and for a transonic wing/body code validation experimental program that currently is conducted within GARTEUR (AD) 28. For the present validation study a both design and an off-design flow case have been selected for which (limited) experimental data is available from previous experimental studies carried out in the ONERA S1-Modane wind tunnel (Ref 5). The design condition test case has also been included in the EC funded program AVTAC (Ref 1). The AVTAC project, however, was aimed at the improvement of solution techniques and turbulence models and concentrated less on a detailed comparison with experiment and in between CFD methods. In this paper a detailed comparison is presented of the computational results including pressure distributions, skin friction distributions and boundary layer velocity- and turbulence profiles.

2 Test cases

The AS28G wing-fuselage transport aircraft model of AS has been selected as a well-suited geometry for the CFD validation study. The wind tunnel model has been tested in the ONERA S1-Modane wind tunnel (Ref 5). This is a half model at 1/7.5 scale, and the model consists of a fuselage, a wing (representative for modern transport aircraft), a wing-fuselage-fairing



(Karman), and a leading edge fairing at the wing root (onglet). From the experimental program two test cases have been selected for the present validation study.

The first test case (referred to as Case 1) is at the design condition of the configuration, being a free stream Mach number of 0.8, and an angle of attack of 2.2 degrees. In the experiment a Reynolds number of $10.6 \cdot 10^6/m$ has been realised. At this condition a shock wave of moderate strength is observed on the wing upper surface, but the flow is still attached showing only a mild tendency towards separation at the wing trailing edge.

A second test case (referred to as Case 2) has been defined for an off-design condition with again a free stream Mach number of 0.8 but now at an angle of attack of 2.57 degrees. The experimental Reynolds has been $11.0 \cdot 10^6/m$. At this condition the flow shows incipient (weak) shock induced flow separation on the wing upper surface and some more separation close to the wing trailing edge. It should be mentioned here that it has been decided to use a free stream Reynolds number of $11.0 \cdot 10^6/m$ for both test cases.

The wind tunnel experiment has been carried out for a half model mounted at the test section wall where the walls were ventilated. Due to uncertainty about the wind tunnel wall effects, and the inability of the CFD methods to properly model the ventilated walls it has been decided to carry out the computations for 'nominal' flow conditions in free air. In the experiment boundary layer transition has been forced by applying transition strips. For the wing transition was enforced at approximately 7% chord position for the wing, and for the fuselage at a distance of 75mm from the nose of the fuselage. Finally, it should be noted that in the experiment the model deformations were known for only a limited number of loads. It has been decided to use the non-deformed wind tunnel geometry that was designed to match the real flight shape at the design flow condition.



3 CFD Methods

All methods employed by the participants within the Action Group solve the Reynolds-averaged Navier-Stokes (RaNS) equations on block-structured meshes. General information on the various CFD methods used by the participants can be found in the following list of references.

Table 1 The CFD methods and the spatial discretisation schemes they use

Parti- pant	Ref	Acronym	Spatial discr.
AS	Ref 13	NSMB	CC-CD
BAe		RANSMB	CC-CD
DASA	Ref 10	FLOWer	CV-CD
NLR	Ref 8	ENFLOW	CC-CD
ONERA	Refs 3, 4	CANARI	CC-CD
Saab	Refs 11, 12	Multnas	CC-CD

CC: Cell Centered CV: Cell Vertex CD: Central Differencing

With this similarity in the spatial discretisation of the various methods the possible differences between solutions should be related to either implementation details, and more specifically the way that artificial dissipation is introduced in the schemes, or the turbulence models employed by the methods. Some details on the artificial dissipation for the CFD methods are listed below.

- AS anisotropic 2nd and 4th order with Mach number damping normal to solid walls
- BAe anisotropic 2nd and 4th order, scaled by mesh Reynolds number
- DASA anisotropic 2nd and 4th order
- NLR matrix (normal to solid walls) and anisotropic 2nd and 4th order
- ONERA anisotropic 2nd and 4th order
- Saab anisotropic 2nd and 4th order with Mach number damping normal to solid walls

It should be noted that the qualification anisotropic is referring to a cell aspect ratio scaling which is commonly adopted in cell centred schemes in case of viscous flow simulations. It should be noted that for truly grid-converged solutions the effects of the artificial dissipation terms should be negligible. There are also some differences in the solution techniques employed to integrate the equations to a steady state. But since all flow solutions are considered to be well converged, these differences should not show up in the computational results.

The various turbulence models that have been used by the participants are listed in the following table.

Table 2 Turbulence models

Partici- pant	Model	Reference	Transition
AS	B&L*	Ref 2	fully turb.
BAe	$k - g$	Kalitzin, Ref 7	fixed
DASA	$k - \omega$	Wilcox, Ref 14	fully turb.
NLR	B&L*	Ref 2	fixed
NLR	$k - \omega$	Wilcox-Kok, Ref 9	fixed
ONERA	$k - \omega$	Wilcox, Ref 14	fully turb.
Saab	$k - \varepsilon$	Chien	fixed
Saab	$k - \omega$	Wilcox, Ref 14	fixed

*) B&L : Baldwin&Lomax

Note that, although in the wind tunnel experiment a transition strip has been applied on the model, some of the participants did treat the test cases as fully turbulent flow cases.

4 Computational grid

A common computational grid is used for the computations. The grid has been generated and distributed by BAe. With respect to the dimensions and the density, the computational grid was designed as being representative for present day project type of work in aircraft industry using CFD methodology. The grid is a block-structured grid consisting of 96 blocks with a total number of 2,518,528 cells, and is dimensioned such that it contains four multi-grid levels. The far field boundary is located at three semi-spans from the geometry. Near the wing the grid has a C-C type of topology.

Around the fuselage a C-O topology is adopted (O in the circumferential direction), where the outer grid is of an H-H topology. An impression of the computational grid is given in Fig 1.

The resolution in the viscous regions is such that more than 20 points are located inside the boundary layers over a large part of the geometry. The distance of the first grid point in surface



normal direction is such that the non-dimensional distance scaled by the dimensionless friction velocity (y^+) is close to 1 almost everywhere on the geometry.

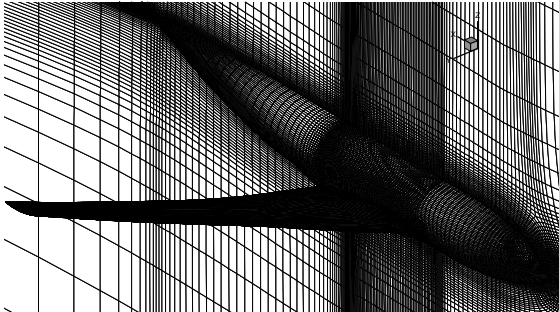


Fig 1 Computational grid on the AS28G geometry and in the symmetry plane

It should be mentioned here that for practical grid generation purposes, the fuselage rear end is left open and extended downstream of the fuselage rear end by a kind of lozenge shaped sting. All participants treat the part of the surface downstream of the fuselage rear end as true symmetry plane, which will probably lead to differences in computed and experimental values for the drag coefficients, due to incorrect pressure distributions close to the fuselage rear end.

5 Discussion of results

Within the Action Group the results of the CFD methods for both test cases have been compared in detail. This comparison consists of

- aerodynamic coefficients (also available from the experiment),
- pressure distributions for the wing upper- and lower surface, and fuselage,
- sectional pressure distributions at seven wing sections for which experimental data is available (see Fig 2), and five fuselage sections,
- skin friction distributions and limiting surface streamlines for the upper- and lower wing,
- sectional skin friction distributions for the wing sections displayed in Fig 2,
- Boundary layer profiles at 12 wing upper surface and near wake stations (grouped into three sections, see Fig 2) for the velocity components, the turbulent viscosity, and the turbulent kinetic energy.

With only limited experimental data available so far the emphasis is on the code to code comparison. New experimental data for this configuration is to be expected from the work of GARTEUR (AD) AG-28. The stations at which boundary layer data are compared are such that they partly coincide with the stations where boundary layer measurements are envisaged within AG-28 (see Fig 2).

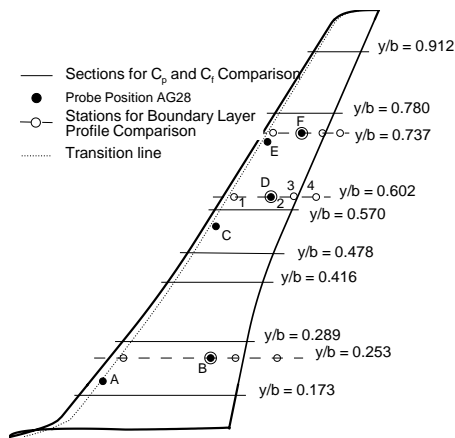


Fig 2 Definition of the wing sections and stations for the AS28G configurations for purpose of comparison of data

The large number of detailed comparisons provided the participants with useful information on the validity and performance of their CFD methods for transonic flow around transport aircraft. In the present paper only a selection of the most critical comparisons is presented which support the main conclusions of the validation study of AG-26. For the full comparisons the reader is referred to the final report of the Action Group (Ref 16).

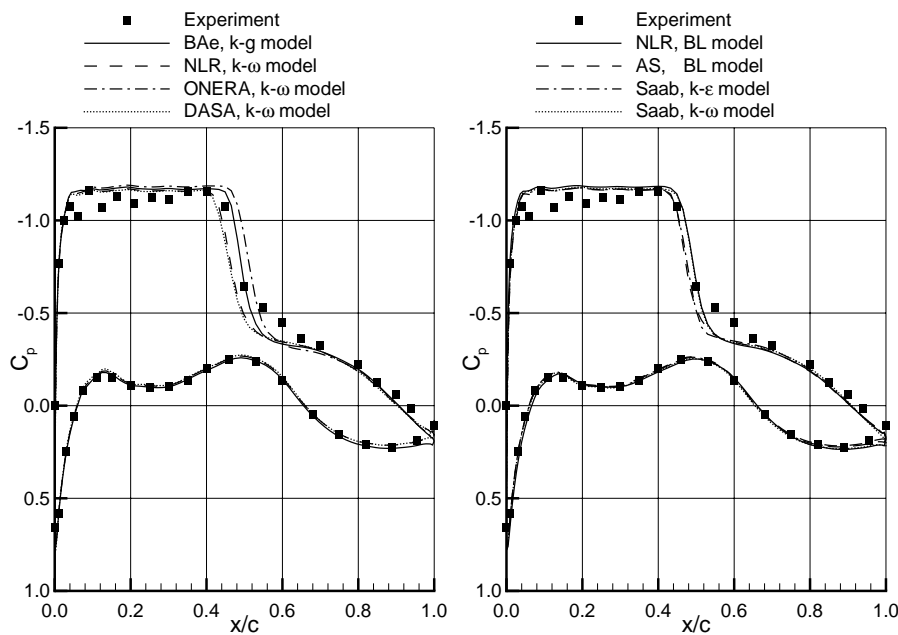


Fig 3 Comparison of pressure distributions for Case 1 (design) of the AS28G configuration at the 57% span wing section



5.1 Pressure distributions

In Fig 3 computed and experimental pressure distributions are compared for a wing section at 57%span (see Fig 2 for the section locations). The pressure distributions on the lower side of the wing are in good agreement with the experiment. The agreement between the different flow solvers in this region indicates that the numerical accuracy issues (like artificial dissipation) can be excluded from the comparison, at least for the regions where the flow is nearly inviscid. The CFD methods agree well with each other upstream of the shock wave, but the pressure coefficient level is slightly lower than in the experiment. This may indicate still some tunnel wall interference, although that effect was supposed to be included in the corrected angle of incidence used for the computations. The computed shock position, show considerable variation among the methods. At this specific station the shock position is best predicted in the BAe ($k - g$), the AS (BL), and the Saab ($k - \epsilon$) results. All methods show a tendency towards flow separation at the trailing edge. Close to the trailing edge all methods fail to match the experimental trailing edge pressure. This is thought to be attributed to deficiencies in the methods (and more specifically the turbulence models) to predict flow separations in an accurate way. The same feature can be seen in the pressure distributions for the off- design case (Case 2) that are presented in Fig 4 for the 57% span wing section.

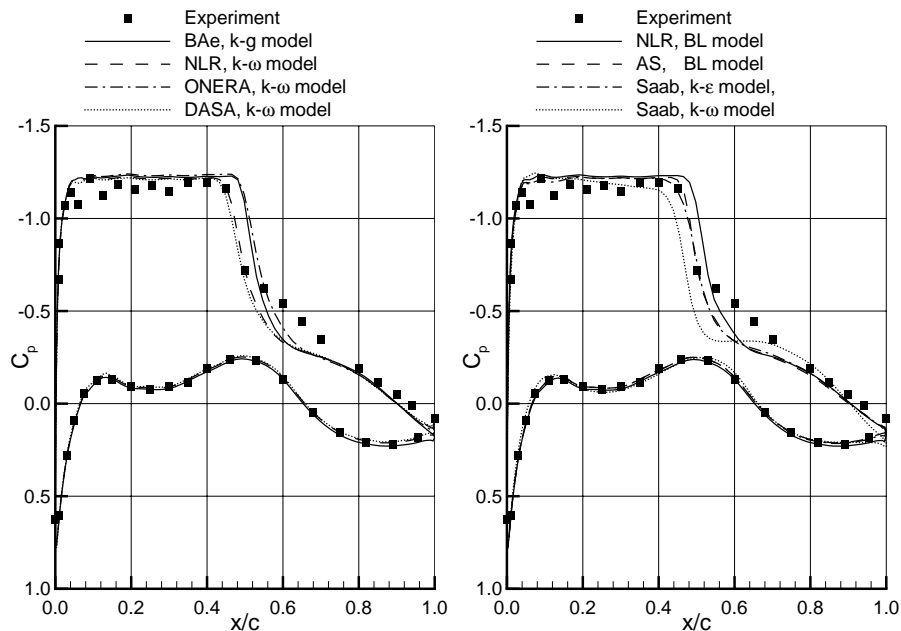


Fig 4 Comparison of pressure distributions for Case 2 (off-design) of the AS28G configuration at the 57% span wing section

For this case the shock position is best predicted by NLR ($k - \omega$) and ONERA ($k - \omega$) at this section. It becomes also more noticeable for the off-design case that the methods fail to predict the pressure distributions downstream of the shock. All methods, except for the Saab ($k - \epsilon$), do predict flow separation but most probably not in the same way as it shows up in the experiment. Based on the differences in numerical schemes, turbulence models and the way boundary layer transition is handled, some pair-wise comparisons can be made. First of all differences in numerical schemes using the same ($k - \omega$) turbulence model (DASA and ONERA) seem to lead to different shock-locations. The $k - \omega$ models of DASA and NLR, that are different in their formulation, predict almost the same shock position.

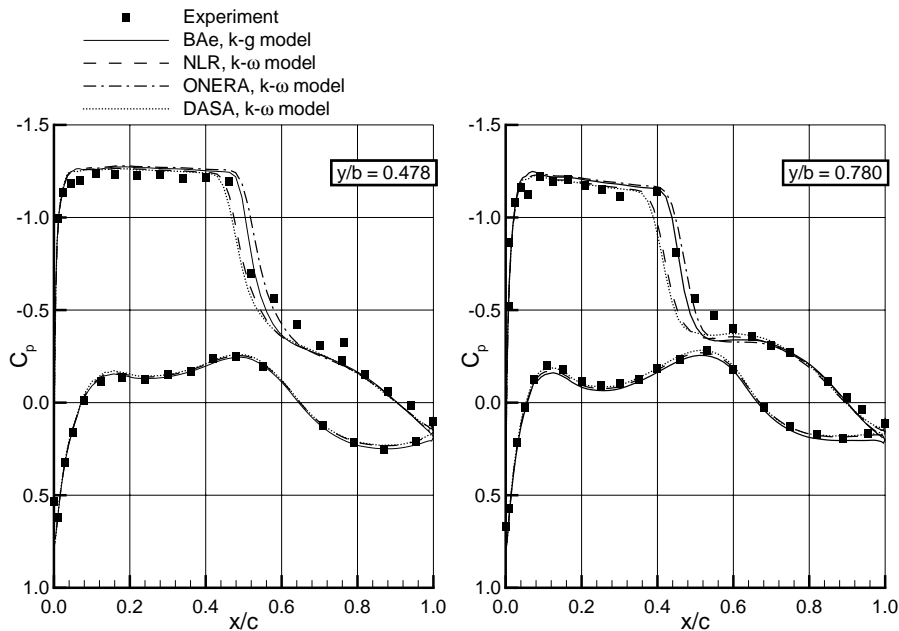


Fig 5 Comparison of pressure distributions for Case 2 (off-design) of the AS28G configuration at the 47.8% and 78% span wing sections

The $k - \epsilon$ model (Saab) seems to predict the shock location more or less the same as the BL model (for Case 1 close to the NLR result, and for Case 2 close to the AS result), and in all cases further downstream than the $k - \omega$ model.

Nor the use of fixed transition or the assumption of fully turbulent flow seems to influence the shock location for the two equation turbulence models. For the BL model results the differences in shock location are most likely caused by differences in implementation rather than by the transition handling.

Finally, in Fig 5 the pressure distributions of some of the solutions are for Case 2 compared with the experimental data at two different spanwise sections. As can be seen the methods that predict the shock position best at the 47.8% span section, NLR and DASA, show a too far upstream shock position (compared to the experiment) at the 78% span section. It is concluded



that when moving from root to tip in spanwise direction the computed shock positions (for all methods) move upstream compared to the experimental shock location. This observed tendency would lead to the conclusion that in spanwise direction the effective angle of incidence varies in a different way in the CFD results than in the experiment. Obviously there is some effect of model deformation (twist) that has not been accounted for in the geometry used for the computations.

5.2 Skin friction distributions

Skin friction is a much more sensitive quantity than the pressure distributions due to the fact first derivatives of the primary flow variables are involved. As can be seen in Fig 6, the skin friction distributions show indeed a larger variation among the CFD methods. The effect of transition handling shows up close to the leading edge.

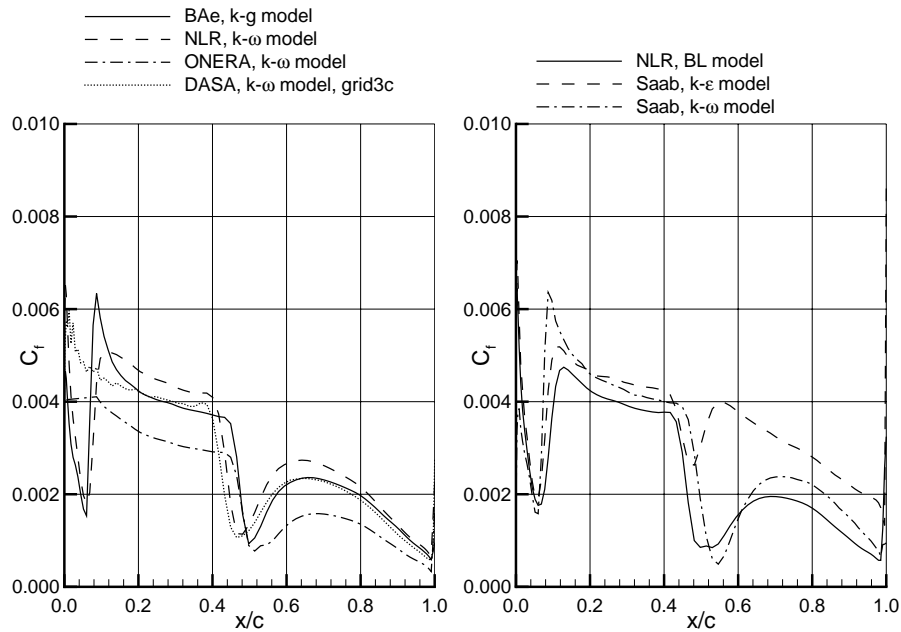


Fig 6 Comparison of skin friction distributions for Case 1 (design) of the AS28G configuration at the 57% span wing sections

The methods that use a fixed transition still differ in the way the turbulence is ‘turned on’ (instantaneously, or smoothly over a number of grid cells) and that difference lead to differences in slope and maximum value downstream of the transition location. After the shock the skin friction sharply decreases and the minimum is a measure for the flow separation. The variation of the location in skin friction drop correlates well with the differences in shock location predicted by the different methods. The level of skin friction predicted by the ONERA method ($k - \omega$) is rather low compared to the other methods. The different ONERA ($k - \omega$) results are



most probably caused by the boundary condition for ω at the no-slip boundary using skin friction velocity, which strongly depends on the wall normal mesh point distribution. A different boundary condition following Zheng et al. (Ref 15) has been implemented since the end of the computations for this action group and has shown improved skin friction distributions (see Ref 16). Despite the differences the general trends in skin friction distribution moving from leading to trailing edge show much similarities among the methods except for the $k - \epsilon$ model results in which the skin friction recovery downstream of the shock is largely over predicted, and the flow does not come close to flow separation like in the other computational results. In Fig 7 upper surface limiting surface streamlines (integrated friction lines) are shown for Case 2 (off-design). As can be seen all results, except for the $k - \epsilon$ model results of Saab show shock induced flow separation along part of the wing span.

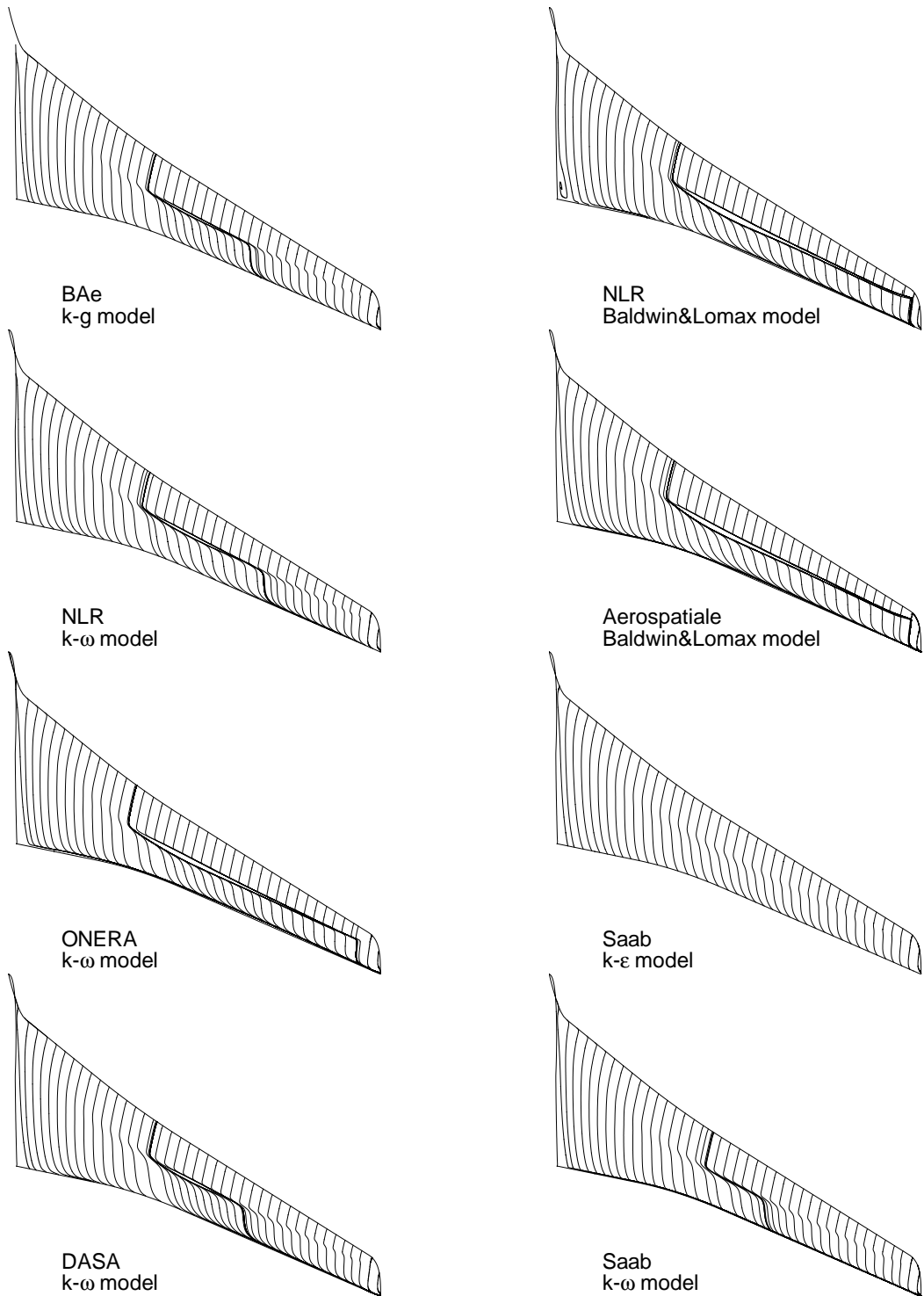


Fig 7 Comparison of upper surface limiting streamlines for Case 2 (off-design) of the AS28G configuration

The Saab ($k - \omega$) result demonstrates the weakest flow separation, which may better be classified as incipient flow separation. Remarkably, the results obtained with the algebraic BL

turbulence model show the largest region of flow separation (for both NLR and AS). Detailed investigation of the region of flow separation (Ref 16) show that the BL model results also show the largest extent of the flow separation region in surface normal direction. This seems contrary to the well-known experiences with the BL model for two dimensional flow where usually, often falsely, separation is indicated by negative values of the skin friction coefficient but with region in which backflow occurs is only restricted to the first two or three grid cells in surface normal direction. Probably the fact that the shock wave position is predicted more downstream by the BL method leads to an increase in shock strength and is causing this larger separation. On the other hand, it seems that the predicted flow separation does not influence the shock position (which normally would move more upstream). The ONERA ($k - \omega$) result show an equally large area of flow separation as the BL model results but this may be due to the boundary treatment as mentioned above. The fact that with the $k - \epsilon$ model no flow separation is predicted for this case is in line with the observation that the model is nowadays recognised as generally over-predicting skin friction for aerodynamic applications. The other three two-equation models, NLR $k - \omega$, BAe $k-g$, and DASA $k - \omega$, predict quite similar flow separation patterns.

5.3 Boundary layer profiles

Boundary layer profiles for the streamwise velocity component and the turbulent viscosity coefficients are presented in Figs 8 and 9. The profiles shown are for the off-design case (Case 2), and for the positions D2, D3, D4 as indicated in Fig 2. For the stations on the wing upper surface the quantities are plotted against the normal distance to the wall (taken along a gridline), where for these stations a logarithmic scale is used. For the wake stations the quantities are plotted against the vertical co-ordinate which is taken zero at the wake plane position in the computational grid.

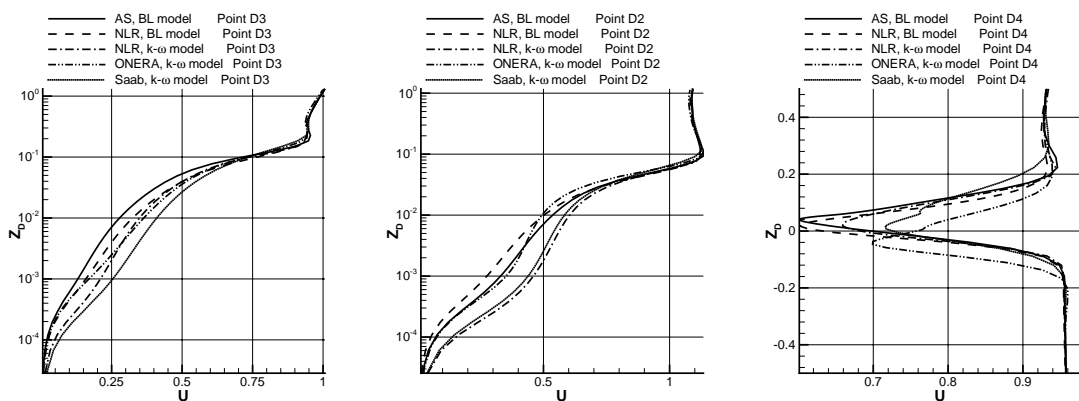


Fig 8 Comparison of streamwise velocity distributions in the boundary layer and the near wake for Case 2 (off-design) for the AS28G configuration

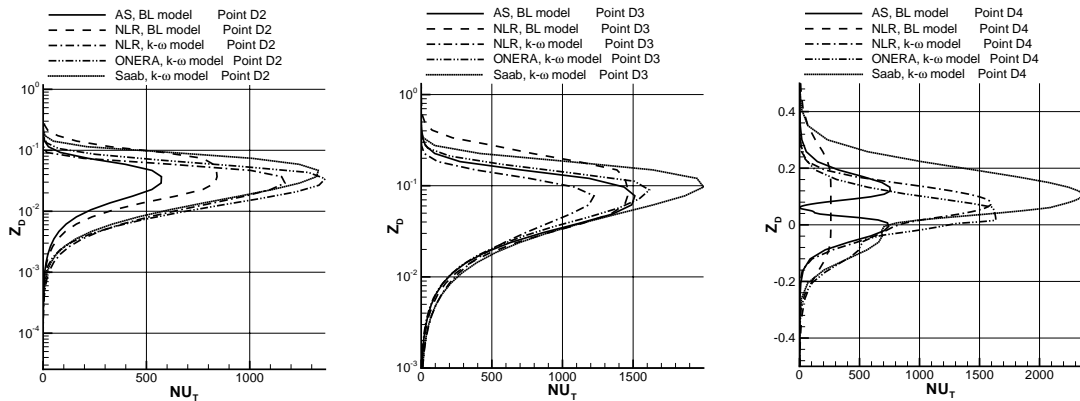


Fig 9 Comparison of turbulent viscosity distributions in the boundary layer and the near wake for Case 2 (off-design) for the AS28G configuration

The boundary layer profiles for the streamwise velocity component at station D2, which is immediately downstream of the shock location show a clustering of the methods that predict the larger flow separation, namely the BL results of NLR and AS, and the $k - \omega$ result of ONERA. At the boundary layer edge (this holds for all stations) all methods agree very well. Moving towards the trailing edge position, D3, it seems that the scatter in boundary layer profiles close to the surface can no longer systematically related to the type of method or the turbulence model used. The largest scatter is observed at the wake station (D4). Most methods seem to agree on the vertical position of the wake (except for the ONERA $k - \omega$ results), but the minimum velocity in the wake profile is quite differently predicted by the various methods. On this point there is again a clear difference between the results obtained with the algebraic BL turbulence model and the results obtained with the $k - \omega$ models. The wake formulation (if used) for the BL model is recognised to under-predict the turbulent viscous effects in the wake region.

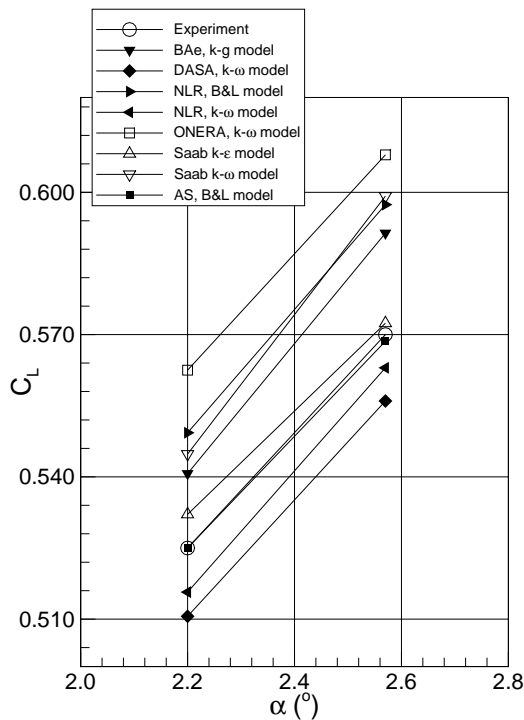


Fig 10 Comparison of computed and experimental lift coefficients for the AS28G configuration

The boundary layer profiles for the turbulent viscosity are less conclusive on the turbulence models used. On the shape of the turbulent viscosity profiles for the wing surface stations all methods agree quite well. The scatter is in the maximum value along the profile, and does not seem to be related to the type of turbulence model that issued. Even the two BL model results show quite some difference in this respect. On the other hand, for the wake station the results again can be grouped according to the type of turbulence model used. The BL model results show remarkably lower values for the turbulent viscosity than the two-equation method results. It seems that AS still applies the ‘inner’ formulation of the model (vanishing turbulent viscosity at the wake centreline where NLR applies the wake formulation). The $k - \omega$ results of NLR, ONERA, and Saab show considerably larger values for the turbulent viscosity in the wake, with the ONERA and NLR grouped together except for the fact that they disagree on the wake position.

5.4 Aerodynamic coefficients

The computed lift-, drag-, and pitch moment coefficients for both cases are presented in Figs 10-12. Most methods over-predict the lift coefficients. Only DASA ($k - \omega$) and NLR ($k - \omega$) under-predict the lift coefficient, which can be explained from the fact that the shock locations are consistently predicted more upstream by these two CFD methods. The computed lift coefficient of AS (BL model) agrees very good with the experimental data for both cases.



Deviations from the experimental values for the lift coefficients are mainly caused by the large variation in the prediction of the shock position. The scatter in lift coefficients can be summarised as

$$C_L^{\text{exp}} - 2.7\% < C_L^{\text{CFD}} < C_L^{\text{exp}} + 7.1\% \quad \alpha = 2.2^\circ, \quad C_L^{\text{exp}} - 2.5\% < C_L^{\text{CFD}} < C_L^{\text{exp}} + 6.0\% \quad \alpha = 2.57^\circ.$$

This scatter is considered as rather large. The slope of the lift curve, however, is quite well predicted by most of the CFD methods except for Saab (both the $k - \omega$ model and the $k - \epsilon$ model).

Except for Saab ($k - \omega$) model all methods under-predict the drag coefficient for both cases (see Fig 11). As mentioned before, the deviations from experiment may partly be attributed to the way the rear part of the fuselage is geometrically modelled in the computational grid. But also from the drag coefficient the scatter of the CFD results is considerable. Deviations from the experimental values of 12% occur for case 1, where for case 2 there is about 10% maximum deviation. In terms of lift over drag, most methods seem to predict the correct slope of the polar where now the result of AS (BL) seems to be over-predicting the drag increment. It is remarkable that despite all deviations in the pressure- and skin friction distributions the result of Saab obtained with the $k - \epsilon$ model, follows the experimental lift over drag polar quite well.

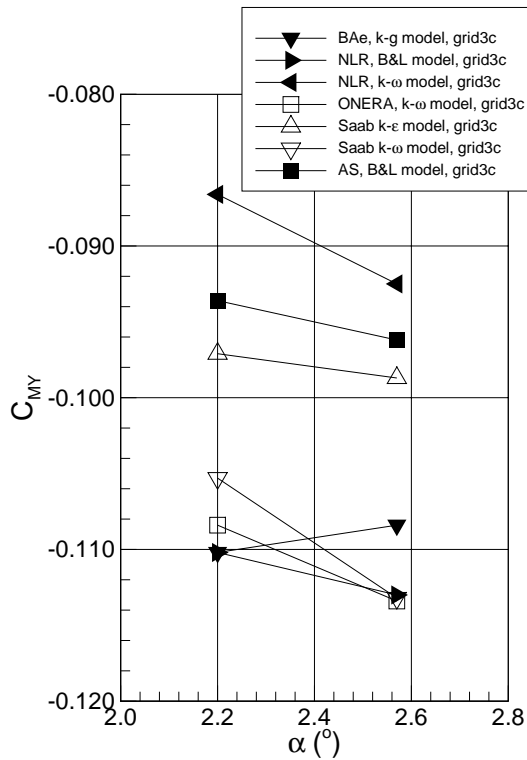


Fig 11 Comparison of computed and experimental drag coefficients for the AS28G configuration

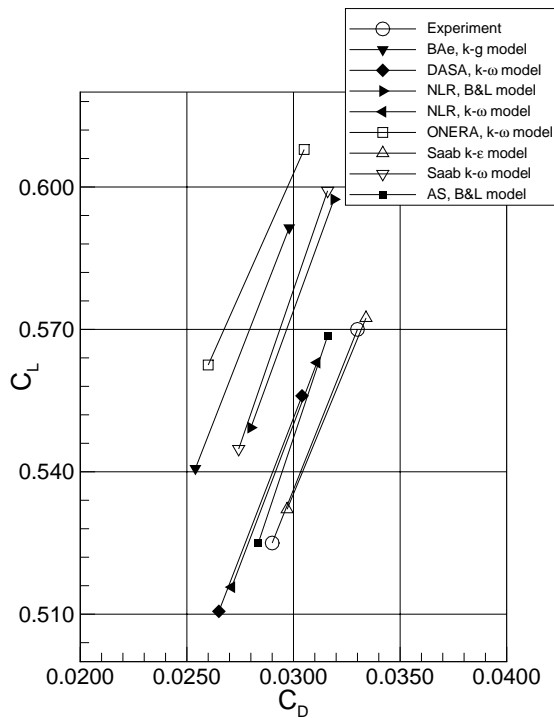


Fig 12 Comparison of computed and experimental pitch moment coefficients for the AS28G configuration

The pitch moment coefficient turns out to be way more sensitive to numerical and modelling errors in the CFD methods than the lift and drag coefficients (see Fig 12). Unfortunately, no experimental values have been made available to AG-26 so far, but the scatter in the computational results would probably lead to the conclusions that no method is capable of predicting the pitch moment in an accurate way. As opposed to lift- and drag coefficients, where the deviations were driven by either only the shock position (lift) or the details of the flow separation (drag), for the moment coefficient it is the combination of both that influences the computed values. It is therefore, that not even agreement on the trend (increase or decrease with increasing incidence) exists among the CFD results. The deviations from the average value are 16.7% and 13% for case 1 and case 2 respectively.

The results for the aerodynamic coefficients can be summarised as follows.

- There is considerable scatter in computed lift- drag- and pitch moment coefficients,
- despite the scatter, most methods predicted the increment in lift for increasing incidence as well as the increment in drag for increasing lift quite good,
- the accuracy of the predicted aerodynamic coefficients does not seem consistently related to the turbulence models employed,



- the scatter in the computed aerodynamic coefficients is of the same order of magnitude for both the design and the off-design case, where one should have expected that the off-design case would be more difficult to compute.

6 Conclusions

The work of the GARTEUR Action Group (AD) AG-26 is presented. The goal of the AG is to analyse the validity of present day CFD methods based on the Navier-Stokes equations for accurate flow computations around transport aircraft. The analysis has been carried out for two transonic flow cases, one design condition and one off-design condition, for the AS28G wing-fuselage configuration. The analysis is restricted to computations on a single common grid of about 2.5 million cells being representative for present day project applications at the sites of the industrial participants. The analysis is based on detailed comparisons of computational and experimental results including aerodynamic coefficients, surface pressure distributions on wing and fuselage, skin friction distributions on the wing, and boundary layer profiles for the velocity components, turbulent viscosity and turbulent kinetic energy.

Based on the comparison with experimental data the following conclusions are drawn

- lift and drag coefficients show considerable deviations from experimental values, although the gradients of the polars (lift vs. incidence, and lift vs. drag) are quite well predicted by most methods,
- pressure distributions correlate very well with experimental data for the lower wing surface,
- upper surface pressure distributions show considerable deviations of the predicted shock position and trailing edge pressures from the experimental data. The correlation of shock location among the CFD results indicates that the wind tunnel model suffered some torsion compared with the computational geometry.

Based on the comparisons between the CFD methods it is concluded that:

- The considerable variation in computed lift, drag, and pitch moment coefficients seem not to correlate with the sophistication of the turbulence model
- Specific choices in the numerical schemes greatly affect the prediction of boundary layer separation
- The Baldwin&Lomax turbulence model predicts shock induced flow separation for both test cases
- The two equation turbulence models fall into four categories,
 - BAe ($k - g$) and Saab ($k - \omega$),
 - NLR ($k - \omega$) and DASA ($k - \omega$),



- Saab ($k - \varepsilon$), of which it is questionable if the model is suitable for computation of external aerodynamic flows,
- ONERA ($k - \omega$) which produces skin friction distributions that became inaccurate due to the boundary condition used for ω ,
- skin friction distributions are rather sensitive to the way transition from laminar to turbulent flow is taken into account, this holds especially for the two-equation turbulence models,
- main differences between the computed boundary layer profiles occurs in the outer part of the boundary layer,
- there is considerable scatter in boundary layer / wake profiles when it comes to maximum/minimum values. This scatter can not be consistently related to the turbulence models applied,
- boundary layer profiles on the wing show in general good agreement in shape for both the velocity and the turbulent viscosity.

It should be noted that the above conclusions are drawn on the basis of comparisons on a single computational grid. In order to be truly able to separate numerical issues from modelling issues (turbulence modelling) a grid convergence study should be executed.

From the detailed comparisons made in this validation exercise the participants gained insight in the performance of their CFD methods. Improvements in both numerical schemes and turbulence modelling are guided by the findings of the analysis performed in AG-26. As an example the work of ONERA on their implementation of boundary conditions can be mentioned in this respect. Also some of the participants developed their CFD methods in such way that model deformations are computed and taken into account during the computations, in order to avoid the some of uncertainties as exposed in the work presented here. When judging the computational results it should be kept in mind that since the work of the AG-26 most participants already improved their CFD methods on a number of issues. Still the work presented here provides a good indication of the potential of CFD methods and more specifically the suitability of turbulence models to compute transonic viscous flow around transport aircraft.

Based on the analysis the following recommendations are made for future validation exercises:

- replace the ‘common grid’ strategy with a ‘grid convergence’ strategy, employing a sequence of grids and resulting into a grid-converged solution for each individual CFD method,
- use more experimental data (envisaged to be obtained from GARTEUR (AD) AG-28),
- clarify the wind tunnel deformation effects as well as the wind tunnel interference effects,
- perform a range of flow condition test cases rather than two isolated cases.

In fact at the moment that this paper is issued there is a GARTEUR Exploratory Group investigating the possibility to continue the work of AG-26 along these guidelines.

7 Acknowledgement

The author wishes to thank the participants of GARTEUR (AD) AG-26 entitled “Transonic wing/body Navier-Stokes computations”, for providing their computational results.

8 References

1. AVTAC, *Revalidation and Industrial Assessment Report*, July 2000. Also available on CD-rom AVTAC/TR/BAE/SM000531.
2. Baldwin, S., Lomax, H. *Thin layer approximation and algebraic model for separated turbulent flow*, AIAA paper 78-0257, 1978.
3. Couaillier V., *Numerical Simulation of Separated Turbulent Flow based on the Solution of RANS/Low Reynolds Two-Equation Model*, AIAA Paper 99-0154, 1999.
4. Couaillier V., Eliasson P., Fassbender J., *Enhancing Robustness for Advanced Turbulence Models in the European Project AVTAC*, AIAA Paper 2000-2407, 2000.
5. *Essais de la demi-maquette AS 28 dans la veine no 1-42,6 m², de la soufflerie SIMA. Partie effet Reynolds. Octobre-Novembre 1984. Etudes 0962 GY 100 G et 3423 AN 043 G*, ONERA-Direction des grands moyens d'essai. Procès-verbal n° 2/0962 GY. Fascicule 2/4. Juin, 1985.
6. GARTEUR (AD) AG-17 : Verification of 3D transonic Euler methods for transport aircraft configurations – Final Report, April 1999.
7. Kalitzin, G., Goulds, A.R.B., Benton, J.J., *Application of two-equation turbulence models in aircraft design*, AIAA paper 96-0327, 1999.
8. Kok, J.C., Spekrijse, S.P. *Efficient and accurate implementation of the $k - \omega$ turbulence model in the NLR multi-block Navier-Stokes system*, presented at ECCOMAS 2000 Conference, Barcelona, Spain, 11-14 September 2000, NLR-TP-2000-144.
9. Kok, J.C. *Resolving the dependence on free-stream values for the $k - \omega$ turbulence model*, AIAA Journal, **38(7)**, 1292-1294, 2000. Also available as NLR-TP-99295.
10. Kroll, N., et al., *FLOWer. Installation and User Handbook, R.115*, DLR Braunschweig, 1998.
11. Lotstedt, P., and Sillen, M., *Multigrid multiblock solver of the stationary Euler and Navier-Stokes equations II*, Saab Report L-0-1 R164, 1996.



12. Sillen, M., *Turbulent flow modelling using EARSM on parallel computers*, TASK Quarterly Vol. 5, No. 2, 247-260.
13. Vos, J.B., Rizzi, A.W., Corjon, A., Chaput E. and Soinne, E., *Recent advances in Aerodynamics inside the NSMB Consortium*, AIAA paper 98-0225, 1998.
14. Wilcox, D.C., *A Two-Equation Turbulence Model for Wall-Bounded and Free-Shear Flows*, aiaa-93-2905, AIAA 24th Fluid Dynamics Conference, Orlando, July 6-9, 1993.
15. Zheng, X., Liao, C., Liu, C., Sung, C.H., Huang, T.T., *Multigrid computations of incompressible flows using two-equation turbulence models: Part 1 – Numerical method*, Journal of Fluid Engineering, **119**, 893-899, 1997.
16. Van der Ven, H., Brandsma, F.J., (eds.), *Navier-Stokes computations of 3D transonic flows for a wing/fuselage configuration, Final report of GARTEUR (AD) AG-26*, GARTEUR TP-127/NLR-TR-2001-341, 2001.